Archives of Environmental Protection
Vol. 50 no. 3 pp. 43–53

PL ISSN 2083-4772
DOI:10.24425/aep.2024.151685

Peganum Harmala seeds extract: A green synthesis route for Mn-doped ZnO nanoparticles as an adsorbent for crystal violet dye removal

Faeza Alkorbi[1]*, Fatima A. Al-Qadri[1,2]

[1]Department of Chemistry, Faculty of Science and Arts at Sharurah, Najran University, Sharurah 68342, Saudi Arabia.
[2]Department of Chemistry, Faculty of Science, Sana'a University, Sana'a, Yemen.

* Corresponding author's e-mail: fhalkorbi@nu.edu.sa

Keywords: Crystal Violet, Mn doping, Adsorption, Nanoparticle, Zinc oxide, *Peganum Harmala*

Abstract: The employment of green synthesized nanomaterials for water pollution prevention is increasing nowadays. Herein, Mn-doped ZnO nanoparticles were synthesized using *Peganum Harmala* seed extract and subsequently used for crystal violet (CV) dye removal from aqueous solutions. The first part of the study describes the preparation of the adsorbent (Mn-ZnO NPs) using a simple coprecipitation method. The surface properties of the material were characterized by Fourier transform infrared spectra (FTIR), scanning electron microscopy (SEM), and X-ray diffraction (XRD). The second part investigates the adsorption of CV dye onto the surface of the prepared Mn-ZnO NPs. Additionally, the isotherm, kinetics, and thermodynamics of the adsorption process were studied in detail. Batch adsorption analysis was carried out by evaluating different parameters, such as the amount of the adsorbent (0.01g to 0.04 g), CV concentration (20 to 80 mg/L), adsorption time (30 to 120 min), and temperature (35 to 65 ºC). The maximum CV dye adsorption capacity of the Mn-ZnO NPs was 45.60 mg/g. The thermodynamic study revealed the spontaneous, exothermic, and feasible nature of the adsorption process, primarily driven by physical forces. Kinetic and isotherm analyses indicated that the adsorption of the dye best fit the Freundlich isotherm and pseudo-second-order models, respectively. Mn-doped ZnO is considered an effective adsorbent for CV, benefiting from its rapid and easy preparation, non-toxic nature, and 94 % adsorption efficiency. The material holds potential for future applications in the removal of organic dyes from wastewater..

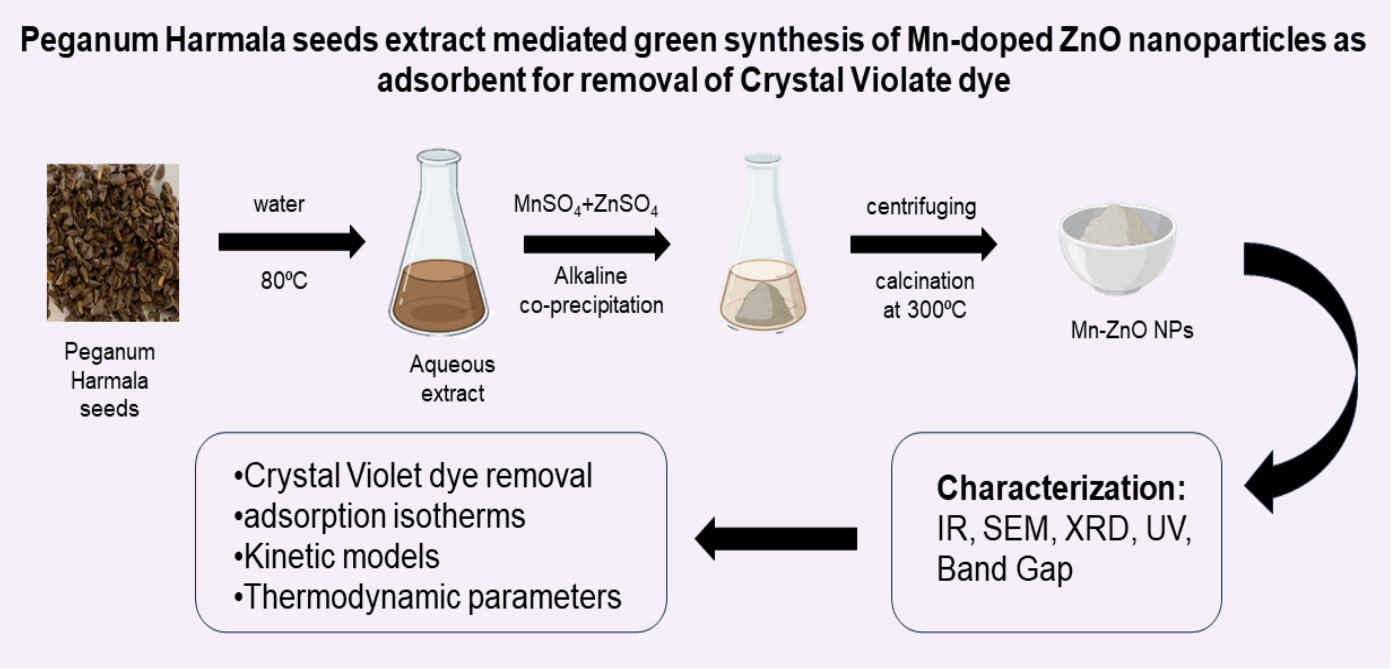

Introduction

Heavy metal ions and synthetic organic dyes harm human health and living organisms, causing environmental pollution. Synthetic organic dyes are widely used in various industries and have become indispensable. Crystal violet (CV), a cationic triphenylmethane dye, is frequently used in various industrial applications. This harmful and toxic material does not break down and causes many serious diseases in humans, including cancer. Long-term exposure to this dye, even in minimal proportions, leads to serious health complications for humans (Homagai et al. 2022). In recent years, growing concerns about water pollution, climate change, limited natural resources, and public health have increased the importance of developing environmentally friendly products and procedures. Adsorption is one of the viable methods to remove dyes from wastewater. It is proven to be an effective strategy because it is simple, inexpensive, and sustainable, allowing the adsorbent to be reused. Adsorption has been widely applied in research to remove organic dyes and heavy metals. The efficiency of the dye removal through adsorption greatly relies on the adsorbent used.

Elimination of dyes from wastewater can be achieved using various adsorbents in adsorption techniques, one of which is nanostructured metal oxides. Metal oxide nanoparticles have proven to be effective adsorbents due to their easy and cost-effective synthesis, requiring minimal quantities for the successful removal of pollutants. Additionally, they are favored for their strength, high surface reactivity, and high adsorption capacity (Kasbaji et al. 2023).

Zinc oxide nanoparticles are among the metal oxides extensively employed as adsorbents due to their distinct chemical, physical, and photocatalytic properties. Additionally, ZnO nanoparticles exhibit extraordinary efficacy in the removal of heavy metal ions and dyes from water-based solutions. The physicochemical characteristics of ZnO nanoparticles can be significantly modified by doping them with a secondary metal element to improve adsorption efficiency and selectivity (Jadoun et al. 2024). Nanobiotechnology, an emerging and rapidly growing field, involves the synthesis of nanoscale materials. Plant extracts are commonly used for this synthesis due to their safety, ready availability, lack of toxicity, and the presence of diverse active phytochemicals, which facilitate the reduction of metallic ions (Aigbe and Osibote, 2024).

Peganum Harmala L., a plant from the Zygophyllaceae family, thrives naturally in North Africa and the Middle East. Its seeds are rich in therapeutic alkaloids, known as harmala alkaloids, as well as anthraquinones, flavonoids, and polysaccharides, Additionally, *Peganum Harmala* possesses a wide array of biological components with antioxidant, antimicrobial, and anticancer activities (Zhu et al. 2022). *Peganum Harmala* L. seed powder has been reported as a green absorbent for heavy metals such as Ni (Ghasemi et al. 2014), Co (Alsaiari, 2022), Fe (Alsaiari et al. 2024), and Cu (Alsaiari et al. 2021). Moreover, the seed extract has been used to synthesize various metals and metal oxides for different applications. Biogenic synthesis of Au, Ag (Ullah et al. 2024), Pt, Pd (Fahmy et al. 2021), CuO (Fekri et al. 2022), and ZnO (Mehar et al. 2019) has been reported using *Peganum Harmala* seeds. The active components, such as harmala alkaloids, anthraquinones, and flavonoids, are responsible for the bio-reduction of various metal ions (Fekri et al. 2022; Mehar et al. 2019).

In this work, *Peganum Harmala* seed extract was used as a green agent in the synthesis of Zinc oxide which doped with 10% Mn ions. The resulting material was applied as an adsorbent to eliminate CV dye from aqueous systems. To derive the adsorption isotherm models and kinetics, the impact of various factors on the adsorption process of CV dye was considered, including adsorbent quantity, contact duration, initial dye concentration, and temperature. The thermodynamic parameters were also determined to assess the viability of CV adsorption onto Mn-doped ZnO.

Experiment

Materials

Peganum Harmala seeds were purchased from a local store. The chemicals, which were of analytical grade and used without any additional treatment, were obtained from Sigma-Aldrich (Germany). These chemicals included crystal violate dye (CV), zinc sulfate heptahydrate ($ZnSO_4.7H_2O$), manganese sulfate monohydrate ($MnSO_4.H_2O$), ethanol, and sodium hydroxide (NaOH). Deionized milli-Q water, obtained from the Millipore-Milli-Q CLX 7080 system (MillporeSigma, USA) was used in the preparation of all aqueous solutions.

Preparing the Peganum Harmala Seeds extract.

Peganum Harmala seeds were thoroughly rinsed with deionized water to eliminate any contaminants and then left to dry in the open air. Ten grams of the dried seeds were weighed and transferred into a round-bottom flask fitted with a condenser, followed by the addition of 100 mL of deionized water. The mixture was heated for 45 minutes at 80 °C. After heating, the mixture was left to cool at room temperature. The *Peganum Harmala* seeds were then removed by filtration, and the aqueous extract was collected and stored at 4 ºC (Fekri et al. 2022).

Synthesis of 10% Mn-doped ZnO

A green method was adopted to prepare the Mn-doped ZnO adsorbent using the alkaline co-precipitation technique with *Peganum Harmala* seed extract. To synthesize the 10% Mn-ZnO catalyst, 7.030 g (24.45 mmoles) of Zn $SO_4.7H_2O$ and 0.4141 g (2.45 mmoles) of $MnSO_4.H_2O$ were added to 100 mL of the *Peganum Harmala* seed aqueous extract. The mixture was stirred with a magnetic stirrer for 2 hours at ambient temperature. Then, 2M NaOH was added gradually until the pH was adjusted to 11, monitored using a digital *p*H meter (model 744, Metrohm AG, Switzerland) equipped with a combined glass electrode. The resultant precipitate was subjected to centrifugation, followed by two washes with deionized water and ethanol. Subsequently, it was dried at 80°C in an oven for 24 hours. The powdered sample was then calcined at 300°C for 3 hours (Lemecho et al. 2022).

Characterization of Mn-Doped ZnO Nanostructures

The surface morphology and elemental composition of Mn-ZnO nanoparticles (NPs) were investigated using a JEOL JSM-7600F Field Emission Scanning Electron Microscope

(JEOL, Japan). Fourier transform infrared (FT-IR) spectroscopy was performed using a 100 FT-IR Spectrometer (Perkin Elmer, USA) to determine the functional groups within the wavenumber range of 400 to 4000 cm^{-1}. The crystallographic arrangement of Mn-doped ZnO was examined using an X'Pert Pro powder X-ray Diffractometer (Malvern PANalytical, UK). Optical absorption was measured at room temperature using a GENESYS 10S UV-Vis Spectrophotometer (Thermo Fisher Scientific, USA) in the wavelength range of 200-800 nm.

Dye adsorption experiments

The following batch adsorption tests were performed: In a conical flask, 25 mL of a stock solution containing 40 mg/ L of the crystal violet (CV) dye was added. The solution and a set quantity of adsorbent (0.02 g) were then stirred at room temperature for 60 minutes. The supernatant underwent centrifugation at 2000 rpm. The quantity of crystal violet dye adsorbed onto the sorbent and the removal percentage were determined using the equations provided below (Ahmadi & Ganjidoust, 2021; Kumar & Kirthika, 2010; Paksamut & Boonsong, 2018).

$$q_e = \frac{(C_0 - C_e)\ V}{w}$$

$$\%R = \frac{(C_0 - C_e) \times 100}{C_0}$$

Where, q_e is the adsorption capacity measured in mg/g, while C_o and C_e represent the initial and equilibrium concentrations of crystal violate dye in water post the removal process (mg/ L), respectively. V stands for the solution volume (L), and W corresponds to the amount of Mn-doped ZnO adsorbent used (g). The adsorption efficiency (%R) was used as the analytical response. To achieve optimal results, the study explored the influence of Mn-doped ZnO dosages (0.01, 0.02, 0.03, and 0.04 g), initial CV concentration (20, 40, 60, and 80 mg/L), exposure time (30, 60, 90, and 120 min), and temperature (35, 45, 55, and 65 ºC).

Results and discussion

Characterization of Mn-ZnO

Figure 1(a) shows the X-ray diffraction pattern of Mn-doped ZnO nanoparticles. The figure illustrates several diffraction peaks, indicating the polycrystalline nature of the synthesized powder. The primary diffraction peak was recorded at 36.34º corresponding to the reflection peak of (101) according to ICDD card number 79-2205 for the hexagonal ZnO phase. ZnO exists in three phases: cubic Zinc blende, hexagonal Wurtzite, and rock salt phases (Shaba et al. 2021). The hexagonal Wurtzite phase is recognized as the thermodynamically most stable phase among these three, and it is usually obtained as reported by many authors (Al-Kahlout, 2012; Darroudi et al. 2013; Liu et al. 2002; Sriram et al. 2017; Theyvaraju & Muthukumaran, 2015; Yildirimcan et al. 2016). The other two phases are considered metal-stable phases which need special conditions for preparation.

The deposited powder shows a preferred orientation in (101) direction as recorded. The other diffraction peaks are indexed to different planes, as shown in Figure 1. The three strongest

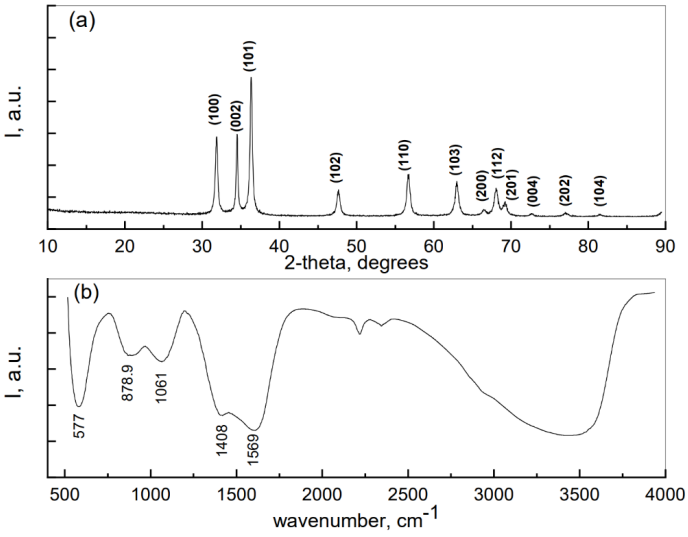

Figure 1. (a) XRD pattern and (b) FT-IR spectra for Mn-doped ZnO nanoparticles.

diffraction peaks belong to the (002), (100), and (101) planes. These high intensities of these planes are attributed to the low surface free energy of formation. Andrade et al. (Paraguay et al. 1999) revealed that the surface free energy densities of these three planes are 9.9, 12.3, and 20.9 eV/nm^2 for (002), (110), and (100), respectively. No additional peaks related to any other phases, such as copper oxide or manganese oxide, were recorded, confirming the singularity of the ZnO phase and the good solubility of Mn into ZnO. This could be due to the low concentration of Mn, which is below the recorded solubility limit of Mn (30% (Mandal et al. 2006)) in ZnO. Additionally, the similar ionic radii of Mn and Zn facilitate the substitution of Zn by Mn, preventing the segregation of Mn into separate grains (Mn^{2+}(0.8Å (Castañeda et al. 2005)), Mn^{3+}(0.65Å (Trari et al. 2005)) and Zn^{2+}(0.74Å (Aboud et al. 2019)).

Scherer's equation is applied to estimate the crystallite size of the deposited powder (Aboud et al. 2023);

$$D = \frac{0.9\,\lambda}{\beta\cos(\theta)}$$

Where λ denotes the incident X-ray wavelength, β represents the full width at half maximum, and is the center of the diffraction peak, the average crystallite size was found to be 36.5 nm. This value has been documented by Bououdina et al (Bououdina et al. 2014) for Mn-doped ZnO nanoparticles synthesized through the Sol-Gel method. Also, in the work of Mote et al (D. Mote et al. 2013) the crystallite size was found to range from 42.5 to 33.64 nm as Mn content increases.

The lattice parameters (a and c), lattice volume (V), and the Zn-O bond length can be estimated using the following equations (Aboud et al. 2023), (Seetawan et al. 2011);

$$\frac{1}{d^2} = \frac{4}{3}\left(\frac{h^2 + hk + k^2}{a^2}\right) + \frac{l^2}{c^2}$$

$$V = 0.866(ca^2)$$

$$L = \sqrt{\frac{a^2}{3} + \left(\frac{1}{2} - r\right)^2 c^2}\ ,$$

where $r = \frac{a^2}{3c^2} + 0.25$

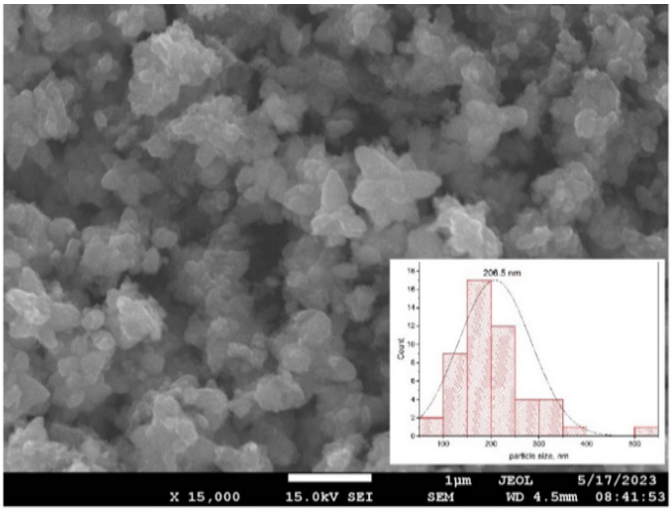

Figure 2. SEM image for Mn-doped ZnO nanoparticle and the statistical distribution of the grain size.

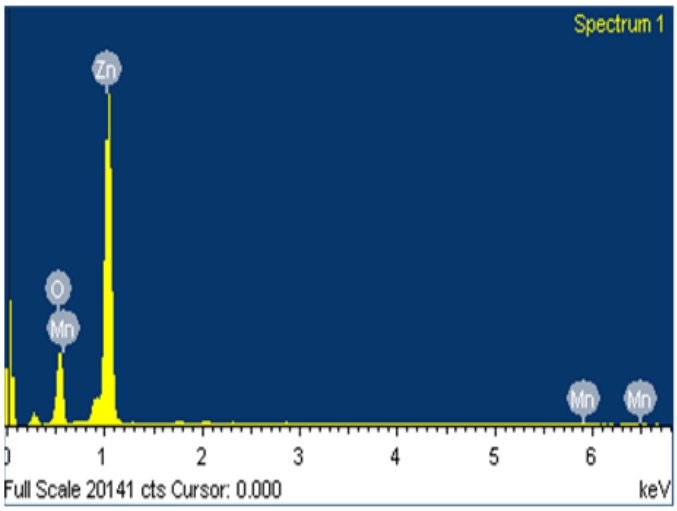

Figure 3. EDX spectrum of Mn-doped ZnO nanoparticles.

The lattice parameters of the prepared powder were found to be a=3.245 Å and c=5.196 Å. These values are slightly smaller than the recorded values in the ICDD card, which are a=3.25 and c=5.2Å. Consequently, the volume is recorded to be 47.398 Å^3, which is smaller than the ICDD value of 47.63Å^3. This reduction in lattice volume can be explained by the replacement of Zn^{2+} with Mn^{2+}, which has a smaller ionic radius. The bond length was found to be 2.01 Å, matching the value of the Zn-O bond in bulk ZnO (Chen et al. 2019).

Figure 1(b) shows the FT-IR spectrum of the deposited Mn-doped ZnO nanoparticles, revealing several absorption peaks. The IR spectrum depends not only on the nature of the material but also on its morphology (Yang et al. 2009). The broad peak between 2970 to 3660 cm^{-1} is assigned to water molecules present in the nanoparticles or adsorbed on the surface (Khan et al. 2011). Weak peaks at 1408 cm^{-1} and 1596 cm^{-1} correspond to the vibrations of symmetric and asymmetric C=O bonds, respectively. Additional bands were detected at below 1400 cm^{-1} associated with Zn-O bond vibrations (Zafar et al. 2019).

The surface morphology, grain size, and chemical composition of the prepared powder have been investigated using SEM and EDX techniques. Figure 2 displays the SEM image of the prepared powder along with the statistical distribution of the recorded grains. The figure shows particles of various shapes with irregular size distribution. The average particle size was measured to be 209.6 nm, significantly larger than the calculated crystallite size obtained from Scherer's equation. This discrepancy could be attributed to the agglomeration phenomena. Figure 3 shows the EDX spectrum, where Zn, Mn, and O peaks are recorded at their regular positions. The elemental ratios of the recorded elements are found to be O:Mn: Zn = 54.62:0.2:45.18.

The UV-Vis spectrometer was employed to examine the optical characteristics of ZnO doped with Mn at room temperature. The analysis revealed a decrease in absorbance with an increase in wavelength, as illustrated in Figure 4. Tauc's relation was then applied to the UV-Vis absorbance data to construct plots for calculating the energy band gap (Eg):

$$(\alpha h\nu)^2 = A\,(h\nu - Eg)$$

Where α is the absorption coefficient, h is Planck's constant, Eg is the optical band gap of a semiconductor, ν is the photon frequency, and A is the proportionality constant. The band gap can be determined by extending the linear portion of the $(\alpha h\nu)^2$ versus hν plot to the X-axis. The point of intersection on the X-axis provides the band gap value. The estimated Eg value of the Mn-doped ZnO is 2.9 eV, as shown in Figure 4, exhibiting a slight decrease compared to the generally acknowledged value. This agrees with the reported values by Ahmed (Ahmed, 2017). It is reported that a higher concentration of Mn in ZnO (Mn>4%) causes a decrease in the optical band (Singh et al. 2016).

Absorption study

Effect of Adsorbent dose

The influence of the dosage of Mn-ZnO on CV removal was studied by varying the dosage from 0.01, 0.02, 0.03, and 0.04 g at an initial CV concentration of 40 mg/L. As shown in Figure 5, Mn-doped ZnO nanoparticles exhibited a rise in removal percentage, achieving 91% removal at a dosage of 0.01 g. There was no additional increase in the amount of Crystal

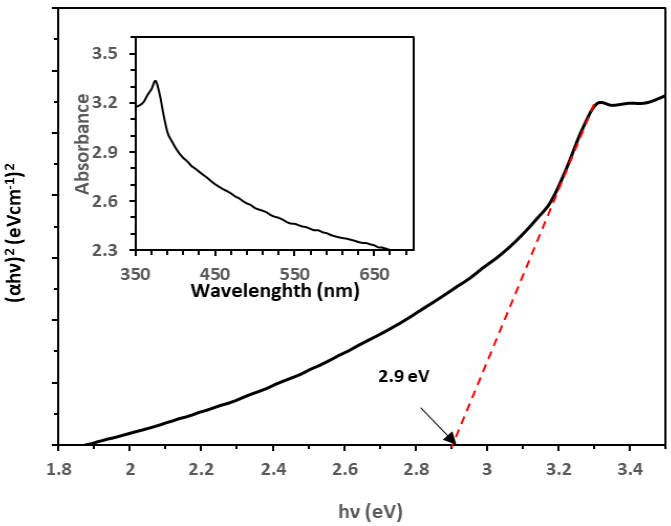

Figure 4. UV spectrum and Energy band gap of Mn-doped ZnO.

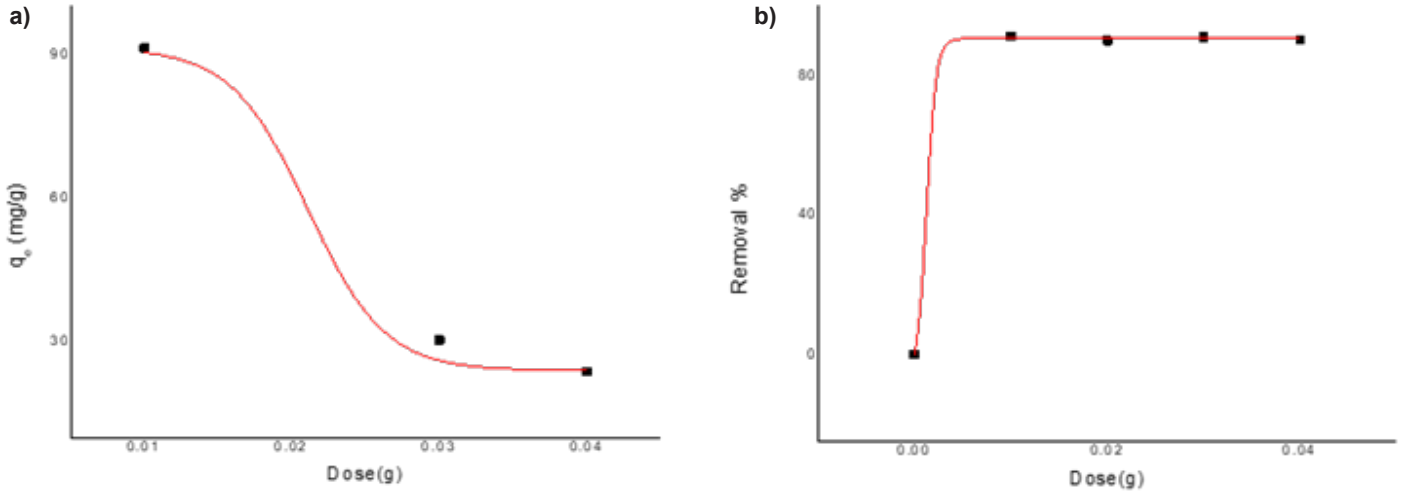

Figure 5. Effect of adsorbent dose on a) adsorption capacity and b) removal efficiency of CV.

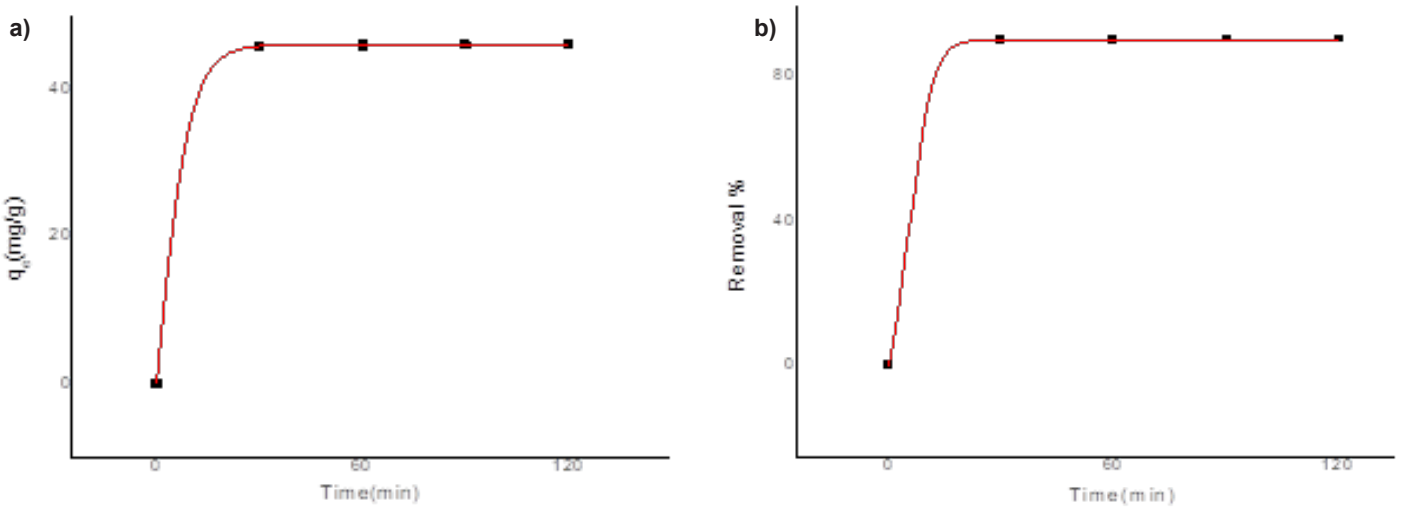

Figure 6. Effect of contact time on a) adsorption capacity and b) removal efficiency of CV.

Violet dye adsorbed when the adsorbent dose was increased beyond 0.01g. The adsorption potential of an adsorbent at a particular starting concentration is largely dependent on the adsorbent dosage. One primary explanation for the variance in adsorption capabilities at different adsorbent doses is the number of accessible adsorption sites. As the dosage increased, the adsorbent's surface area and active sites became more accessible for adsorption. However, once adsorption reached equilibrium, the additional adsorbent dosage induced unavailable sites that did not contribute to further adsorbate uptake (Elsayed et al. 2020). Moreover, the equilibrium concentration of Mn-doped ZnO nanoparticles was lower despite the increased adsorbent dosage, which increased the interference of the adsorbent surface among the active groups. This occurred because there was insufficient driving force for the adsorbate to spread and bind to the adsorbent surface. These results align with earlier investigations (Park et al. 2008).

Effect of contact time

The time needed to achieve equilibrium is a crucial element in the wastewater treatment process. The impact of contact time on CV adsorption on Mn-doped ZnO was investigated at varying times (30, 60, 90, 120 min). Figure 6 displays the results of this effect on CV removal efficiency and adsorption capacity. The findings indicate that the adsorption efficacy for CV and the percentage elimination of CV increased as the contact time increased, reaching equilibrium after 30 min. The abundant pores in the Mn ZnO structure led to a faster transfer of CV mass from the solution onto the material, resulting in faster adsorption at the initial contact. This demonstrates the strong accessibility of adsorbent's CV binding sites, which is favorable for efficient adsorption. Mn-ZnO can bind CV in two different ways. CV can be readily adsorbed by the mesoporous Mn-ZnO material due to the abundant active sites and strong mass transfer driving force in the initial phase of adsorption. However, over time, a significant layer of CV builds up on the surface of Mn-ZnO, limiting the available active sites and obstructing the mobility of CV, leading to nonlinear adsorption. After suitable contact times of 30 and 60 minutes, the highest percentage of CV removal was achieved, reaching 91.20%.

Effect of initial CV concentration

The influence of initial CV concentration (20, 40, 60, 80 mg/L) on the removal efficiency of CV by Mn-ZnO is shown

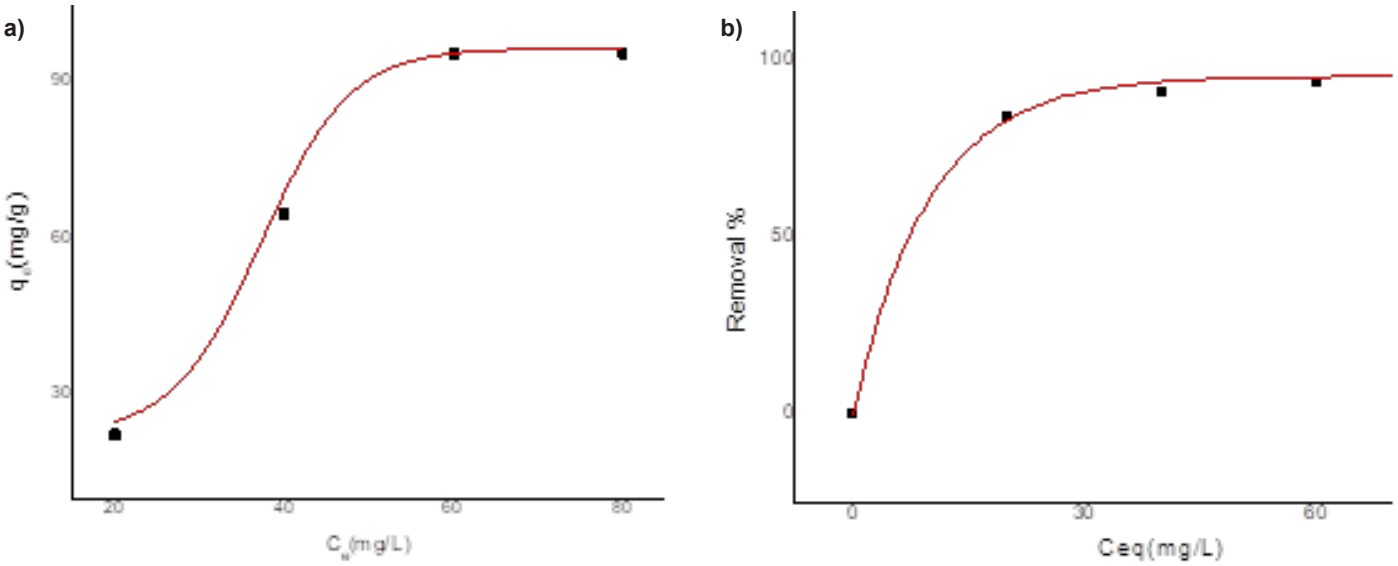

Figure 7. Effect of initial CV dye concentration on a) adsorption capacity and b) removal efficiency of CV.

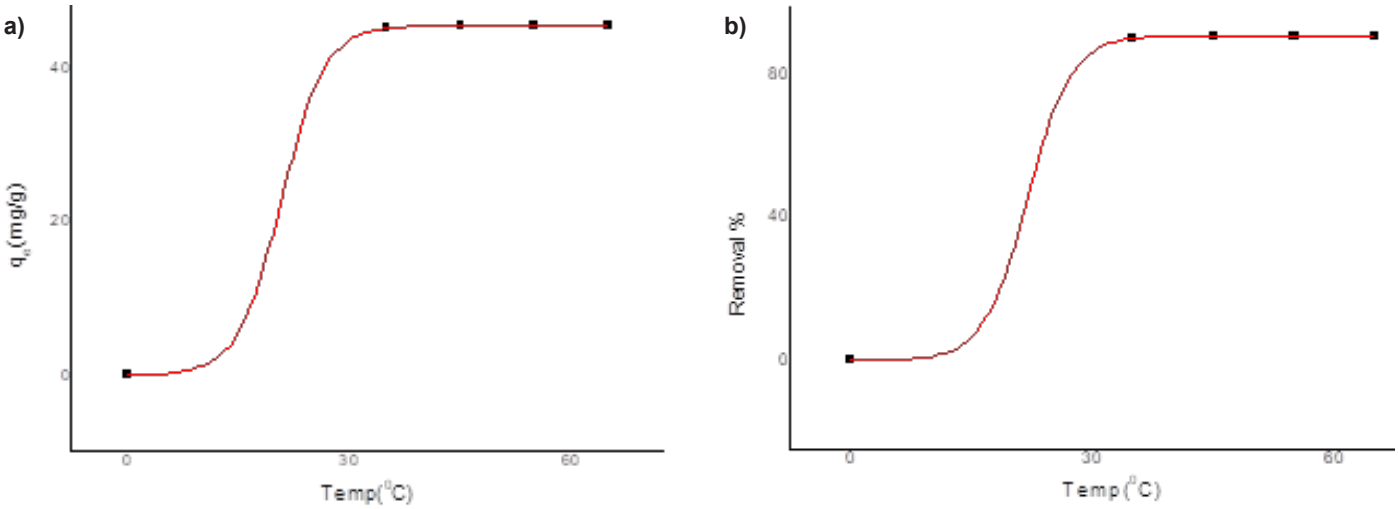

Figure 8. Effect of temperature on a) adsorption capacity and b) removal efficiency of CV.

in Figure 7. The graph indicates that the adsorbed amount increases very marginally with increasing concentrations, exhibiting an upward incline at low concentrations and a steady, flat plateau at higher values. At equilibrium, the adsorption capacity (q_e) rose from 22.24 mg/g to 44.70 mg/g when the initial CV concentration increased from 20 mg/L to 40 mg/L respectively. At a concentration of 80 mg/L, the highest adsorption capacity recorded was 95.14 mg/g. The increase in the initial concentration enhanced the driving power of mass transfer, leading to increased CV adsorption. At an initial concentration of 20 mg/L, the efficiency of CV removal was 94%.

Effect of Temperature

To investigate the impact of the temperature on the adsorption process of CV, experiments were conducted at various temperatures: 35, 45, 55, and 65°C, while maintaining the CV concentration at 40 mg/L. Figure 8 shows that as the temperature increased from 35°C to 45°C, both the percentage removal of CV and the adsorption capacity increased. The amount of CV adsorbed onto Mn-ZnO increased from 45.18 mg/g to 45.53 mg/g. As temperature increased, adsorbent degradation altered the sorbent's surface chemistry, enhancing the accessibility of active functional groups and decreasing CV adsorption. In addition, the increased temperature facilitated the desorption process by altering bond structures (Sharaf & Hassan, 2014). This effect was due to the diminished boundary layer thickness with increasing temperature, which caused metal ions to escape from the surface into the solution phase, limiting the adsorption capacity. Similar findings have been reported by Sharaf and Hassan (2014).

Adsorption Isotherms

The isotherms of the adsorption are produced using the well-known Langmuir and Freundlich isotherm models to identify the appropriate model for optimizing the adsorption processes. The Langmuir isotherm presumes homogenous adsorption, whereas the Freundlich isotherm is an empirical equation

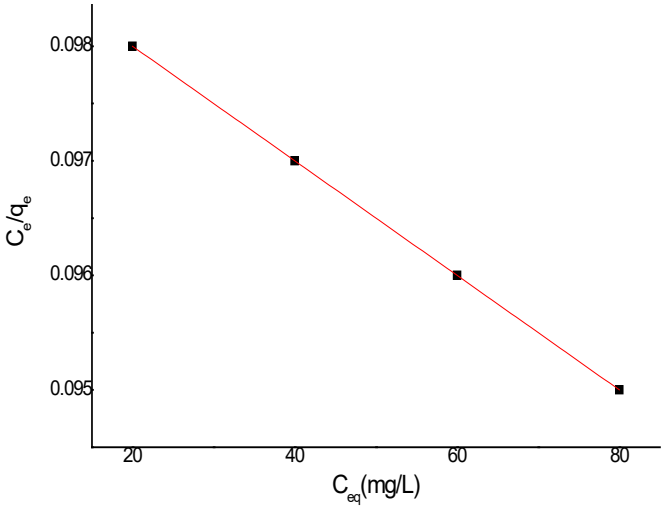

Figure 9. Langmuir isotherm model for adsorption of CV dye on Mn-doped ZnO.

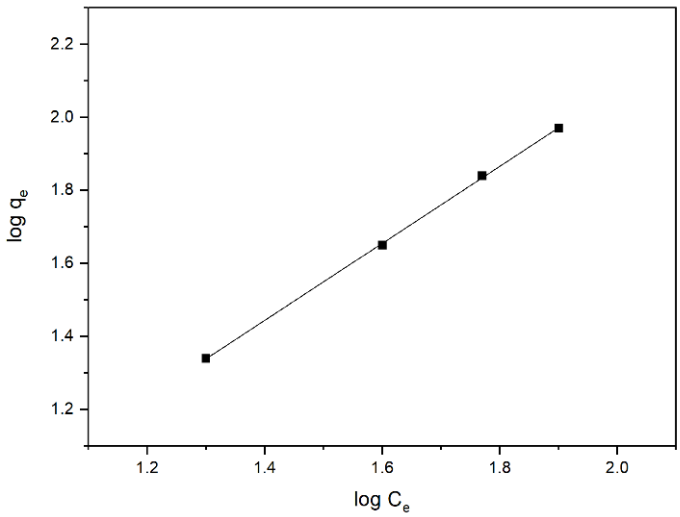

Figure 10. Freundlich isotherm model for adsorption of CV dye on Mn-doped ZnO.

employed to model heterogeneous systems. The Langmuir Isotherm model is presented as:

$$\frac{C_e}{q_e} = \frac{1}{b\ q_{max}} + \frac{C_e}{q_{max}}$$

Where C_e represents the initial CV concentration, q_{max} (mg/g) is the maximum capacity of the monolayer, and b represents a Langmuir adsorption constant. The Langmuir constants b and q_{max} were derived from the slope and intercept (Figure 9). Langmuir isotherm asserts that while undergoing the adsorption process, there is no interaction between adsorbate molecules after the formation of a monolayer (Langmuir, 1916). A dimensionless equilibrium parameter (R_L) can be employed to characterize the fundamental features of the Langmuir isotherm. This parameter's definition is as follows: the adsorption is considered unfavorable when R_L is greater than 1; linear when R_L is equal to 1, favorable when R_L is within the range of 0 to 1, or irreversible when R_L is at 0 (Owoeye et al. 2019). Here, R_L fell within the range of 0–1, signifying the favorable adsorption of CV onto the Mn-ZnO. The monolayer adsorption capacity of CV, as determined by Langmuir isotherm, was 94.3 mg/g.

The Freundlich isotherm is an experimental model that can be represented by the following equation:

$$\log q_e = \log K_f + \frac{1}{n} \log C_e$$

K_f and n are the Freundlich constants, denote the adsorbent's capacity and the intensity of adsorption, respectively, q_e stands for the amount adsorbed per unit of adsorbent at equilibrium (mg/g), and C_e is the concentration of dye at the equilibrium (mg/L). Figure 10 illustrates a linear regression plot log q_e against log C_e, the Freundlich constants K_f and n are easily derived from that plot (Freundlich, 1906). From the Freundlich isotherm, the value of 1/n signifies the favorability of the isotherm type: it is favorable when 1/n is smaller than 1 and unfavorable when 1/n is greater than 1. That accounts for the arrangement of active sites on the surface as well as any element that causes the adsorbent-adsorbate interaction to weaken with increasing surface density.

Table 1 provides the parameters of the Langmuir and Freundlich isotherm models, along with correlation coefficients, for the adsorption of CV on Mn-ZnO. Based on the correlation coefficient R^2 values from the isotherm models, the adsorption data demonstrated better conformity with the Freundlich isotherm (R^2 = 0.99) compared to the Langmuir model (R^2 = 0.92) (Solmaz et al. 2024). Both K_f and n values of the present investigation indicate that CV adsorption on Mn-ZnO is favorable.

Adsorption kinetics studies

The two kinetic models, namely the pseudo-first-order and pseudo-second-order models, were employed to fit the adsorption mechanisms and identify potential rate-determining phases. The solid capacitance is a key factor in the pseudo-first-order model, while the pseudo-second-order model effectively replicates the sorption of analytes from aqueous solutions when chemisorption involves the integration of valence forces. This encompasses the sharing or exchange of electrons between adsorbents and forces (Taha et al. 2017).

Table 1. Adsorption isotherms parameters for CV dye adsorption Mn-doped ZnO.

Langmuir			Freundlich		
q_{max} (mg/g)	*b* (L/mg)	R^2	n	K_f (mg/g)	R^2
94.3	0.0014	0.92	1	0.906	0.99

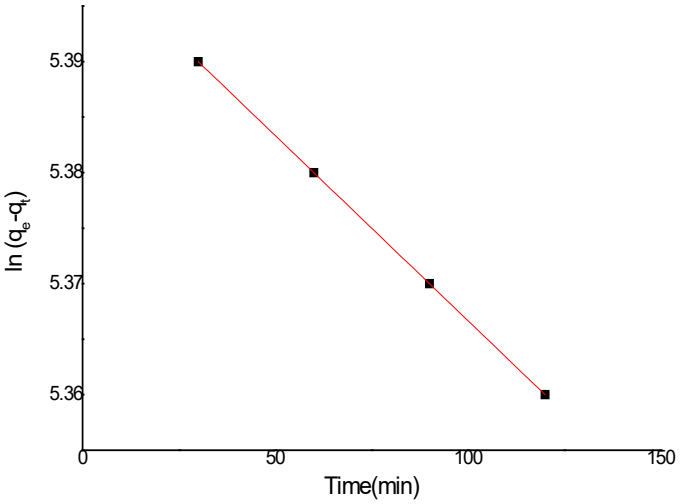

Figure 11. Pseudo-first-order plot of CV adsorption on Mn-doped ZnO.

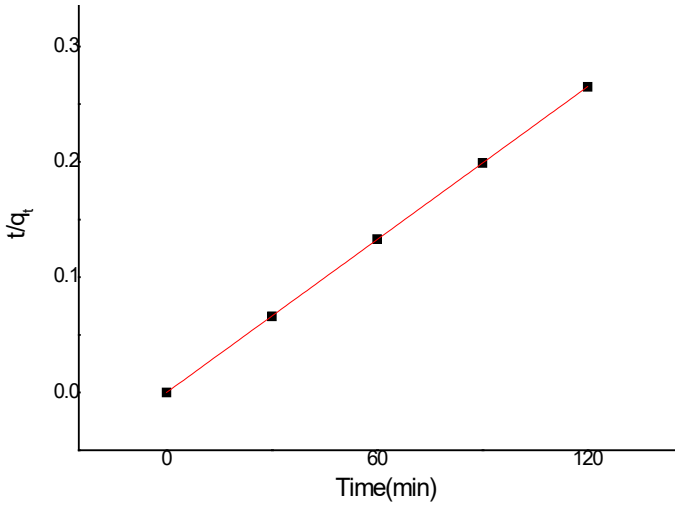

Figure 12. Pseudo-second-order plot of CV adsorption on Mn-doped ZnO.

The following equation can be applied to the pseudo-first-order kinetic model:

$$ln(q_e - q_t) = lnq_e - k_1 . t$$

Here q_i and q_t (mg/g) denote the quantities of CV adsorbed onto Mn ZnO surface at equilibrium and time t, respectively; the rate constant for the pseudo-first-order kinetic model is represented by k_1 (min^{-1}). A linear relationship was achieved by plotting $ln(q_e-q_t)$ against time 't' (refer to Figure 11), and from this linear trend, the rate constant k_1 was determined.

The pseudo-second-order kinetic model is described as follows:

$$\frac{t}{q_t} = \frac{1}{k_2 q_e^2} + \frac{1}{q_e} .$$

Figure 12 displays the standard graph for the fictitious second-order problem.

Table 2 displays the kinetic parameters for the pseudo-first order and pseudo-second order models. The correlation factor R^2 for both models was 0.99. The q_e theoretical value calculated from the pseudo-first-order model varies significantly from the actual observed value, suggesting that this model does not represent the adsorption kinetics. In contrast, the pseudo-second-degree model shows great compatibility with the experimental data for CV adsorption (Gul et al. 2023). The outcomes show that the adsorption of CV by the Mn-ZnO adsorbent is governed by a chemisorption process, with the pseudo-second-order binding mechanism predominating. This process involves valence forces through the exchange of electrons between the dye and adsorbent. A significant affinity exists between CV and the adsorbent, as demonstrated by the short half-adsorption time and the high removal efficiency of CV.

Thermodynamic Parameters

The thermodynamic analysis provides important insights into the adsorption mechanism. Various thermodynamic parameters are obtained to comprehend the adsorption process, such as the changes in the entropy (ΔS°), enthalpy (ΔH°), and free energy (ΔG°). These parameters were determined using the equations below:

$$lnk_d = \frac{\Delta S}{R} - \frac{\Delta H}{RT}$$

$$\Delta G = -RTlnK$$

Based on the slope and y-intercept of the log k_d against temperature (measured in Kelvin) plot in Figure 13, the values of ΔH° and ΔS° are depicted. Table 3 summarizes the information regarding the thermodynamic characteristics associated with the adsorption of the CV process on Mn-doped ZnO. The adsorption is identified as exothermic due to the negative ΔH° value. The ΔS° value was positive, which confirms that the adsorption process occurs randomly at the solid solution interface between Mn-ZnO and CV solution.

Table 2. Kinetic parameters and correlation coefficients for CV adsorption on Mn-doped ZnO. [Experimental adsorption capacity $q_{e(exp)}$ = 45.60 mg/g].

Pesedo-1st order		**Pesedo-2nd order**	
$q_{e,cal}$ (mg/g)	62.95	$q_{e,cal}$ (mg/g)	45.45
k1 (min^{-1})	-0.003	k2 (g/g.min)	0.0026
R^2	0.99	R^2	0.99

Table 3. Thermodynamic parameters for CV adsorption on Mn-doped ZnO.

T (K)	ΔG° (J/mol)	ΔH° (J/mol)	ΔS° (J/mol.k)
308	-2074.18	-0.0024	1.45
318	-317.26		
328	-736.28		
338	- 777.78		

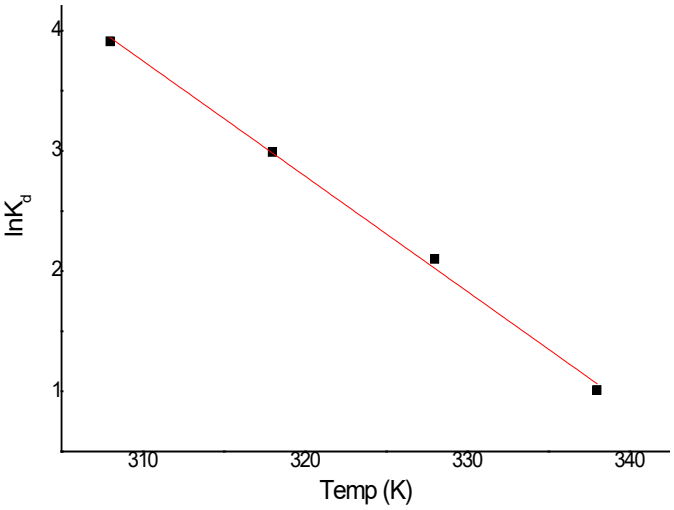

Figure 13. Thermodynamic behavior during the adsorption of CV.

The adsorption process is spontaneous, as confirmed by the negative ΔG° values across different temperatures (Aregawi & Mengistie, 2013).

Conclusion

Current research demonstrates that Mn-doped ZnO is an efficient adsorbent for removing Crystal violet (CV) dye from aqueous systems (%Removal= 91-94%). The synthesis of Mn-ZnO adsorbent was carried out using a sustainable method involving the seed extract of *Peganum Harmala*. Various parameters, including the dosage of adsorbent, initial CV dye concentration, temperature, and contact time, strongly influenced the absorption performance of CV dyes. Compared to Langmuir's model, the Freundlich isotherm model was better adapted for CV dye equilibrium data adsorption (R^2= 0.99). The CV dye adsorption onto Mn-doped ZnO followed the pseudo-second-order model, indicating chemisorption ($q_{e,(cal)}$= 45.45 mg/g, $q_{e(exp)}$ = 45.60 mg/g). The adsorption process was exothermic (ΔH°=-0.0024) and occurred spontaneously (ΔG°< 0), according to thermodynamic calculations. Overall, the findings imply that Mn-doped ZnO can serve as a proficient, green, and sustainable adsorbent for the removal of CV dye from aqueous systems.

Declaration of competing interest

The authors declare that they have no known competing financial or personal interests that could have influenced the work reported in this paper.

Funding

No funding was received for conducting this study.

Acknowledgment

The authors would like to thank the Advanced Materials and Nano-Research Centre (AMNRC), Najran University for carrying out XRD, FTIR, and SEM measurements.

References

Aboud, A. A., Bukhari, Z. & Al-Ahmadi, A. N. (2023). Enhancement of UV detection properties of ZnO thin films via Ni doping. *Physica Scripta*, 98(6), 065938. DOI:10.1088/1402-4896/acd284

Aboud, A. A., Shaban, M. & Revaprasadu, N. (2019). Effect of Cu, Ni and Pb doping on the photo-electrochemical activity of ZnO thin films. *RSC Advances*, 9(14), pp. 7729–7736. DOI:10.1039/C8RA10599E

Ahmadi, S. & Ganjidoust, H. (2021). Using banana peel waste to synthesize BPAC/ZnO nanocomposite for photocatalytic degradation of Acid Blue 25: Influential parameters, mineralization, biodegradability studies. *Journal of Environmental Chemical Engineering*, 9(5), 106010. DOI:10.1016/J.JECE.2021.106010

Ahmed, S. A. (2017). Structural, optical, and magnetic properties of Mn-doped ZnO samples. *Results in Physics*, 7, pp. 604–610. DOI:10.1016/j.rinp.2017.01.018

Aigbe, U. O. & Osibote, O. A. (2024). Green synthesis of metal oxide nanoparticles, and their various applications. *Journal of Hazardous Materials Advances*, 13, 100401. DOI:10.1016/J.HAZADV.2024.100401

Al-Kahlout, A. (2012). ZnO nanoparticles and porous coatings for dye-sensitized solar cell application: Photoelectrochemical characterization. *Thin Solid Films*, 520(6), pp, 1814–1820. DOI:10.1016/j.tsf.2011.08.095

Alsaiari, R. (2022). Removal of cobalt (II) ions from aqueous solution by *Peganum Harmala* seeds. *Indian Journal of Chemical Technology* (Vol. 29).

Alsaiari, R., Alqadri, F., Shedaiwa, I. & Alsaiari, M. (2021). *Peganum Harmala* plant as an adsorbent for the removal of Copper(II) ions from water. *In Indian Journal of Chemical Technology* (Vol. 28).

Alsaiari, R., Shedaiwa, I., Al-Qadri, F. A., Musa, E. M., Alqahtani, H., Alkorbi, F., Alsaiari, N. A. & Mohamed, M. M. (2024). *Peganum Harmala* L. plant as green non-toxic adsorbent for iron removal from water. *Archives of Environmental Protection*, 50(1), pp. 3–12. DOI:10.24425/aep.2024.149894

Aregawi, B. H. & Mengistie, A. A. (2013). Removal of Ni(II) from aqueous solution using leaf, bark and seed of moringa stenopetala adsorbents. *Bulletin of the Chemical Society of Ethiopia,* 27(1), pp. 35–47. DOI:10.4314/bcse.v27i1.4

Bououdina, M., Omri, K., El-Hilo, M., El Amiri, A., Lemine, O. M., Alyamani, A., Hlil, E. K., Lassri, H. & El Mir, L. (2014). Structural and magnetic properties of Mn-doped ZnO nanocrystals. *Physica E: Low-Dimensional Systems and Nanostructures*, 56, pp. 107–112. DOI:10.1016/j.physe.2013.08.024

Castañeda, D., Muñoz H., G. & Caldiño, U. (2005). Local structure determination of Mn2+ in CaCl 2:Mn2+ by optical spectroscopy. *Optical Materials*, 27(8), pp. 1456–1460. DOI:10.1016/j.optmat.2004.10.009

Chen, L., Cui, Y., Xiong, Z., Zhou, M. & Gao, Y. (2019). Chemical functionalization of the ZnO monolayer: Structural and electronic properties. *RSC Advances*, 9(38), pp. 21831–21843. DOI:10.1039/c9ra03484f

Darroudi, M., Sabouri, Z., Kazemi Oskuee, R., Khorsand Zak, A., Kargar, H. & Hamid, M. H. N. A. (2013). Sol-gel synthesis, characterization, and neurotoxicity effect of zinc oxide nanoparticles using gum tragacanth. *Ceramics International*, 39(8), pp. 9195–9199. DOI:10.1016/j.ceramint.2013.05.021

Elsayed, A. E., Osman, D. I., Attia, S. K., Ahmed, H. M., Shoukry, E. M., Mostafa, Y. M. & Taman, A. R. (2020). A study on the

removal characteristics of organic and inorganic pollutants from wastewater by low cost biosorbent. *Egyptian Journal of Chemistry*, 63(4), pp. 1429–1442. DOI:10.21608/ejchem.2019.15710.1950

Fahmy, S. A., Fawzy, I. M., Saleh, B. M., Issa, M. Y., Bakowsky, U. & Azzazy, H. M. E. S. (2021). Green synthesis of platinum and palladium nanoparticles using *Peganum harmala* L. Seed alkaloids: Biological and computational studies. *Nanomaterials*, 11(4). DOI:10.3390/nano11040965

Fekri, R., Mirbagheri, S. A., Fataei, E., Ebrahimzadeh-Rajaei, G. & Taghavi, L. (2022). Green synthesis of CuO nanoparticles using *Peganum harmala* extract for photocatalytic and sonocatalytic degradation of reactive dye and organic compounds. *Main Group Chemistry*, 21(4), pp. 975–996. DOI:10.3233/MGC-220045

Freundlich, H. M. F. (1906). Over the adsorption in solution. *J. Phys. Chem,* 57, pp. 385–471.

Ghasemi, M., Ghasemi, N., Zahedi, G., Alwi, S. R. W., Goodarzi, M. & Javadian, H. (2014). Kinetic and equilibrium study of Ni(II) sorption from aqueous solutions onto *Peganum harmala*-L. *International Journal of Environmental Science and Technology*, 11(7), pp. 1835–1844. DOI:10.1007/s13762-014-0617-9

Gul, S., Afsar, S., Gul, H. & Ali, B. (2023). Removal of crystal violet dye from wastewater using low-cost biosorbent Trifolium repens stem powder. *Journal of the Iranian Chemical Society*, 20(11), pp. 2781–2792. DOI:10.1007/s13738-023-02875-x

Homagai, P. L., Poudel, R., Poudel, S. & Bhattarai, A. (2022). Adsorption and removal of crystal violet dye from aqueous solution by modified rice husk. *Heliyon*, 8(4). DOI:10.1016/j.heliyon.2022.e09261

Jadoun, S., Yáñez, J., Aepuru, R., Sathish, M., Jangid, N. K. & Chinnam, S. (2024). Recent advancements in sustainable synthesis of zinc oxide nanoparticles using various plant extracts for environmental remediation. *Environmental Science and Pollution Research*, 31(13), pp. 19123–19147. DOI:10.1007/s11356-024-32357-3

Kasbaji, M., Ibrahim, I., Mennani, M., abdelatty abuelalla, O., fekry, S. S., Mohamed, M. M., Salama, T. M., Moneam, I. A., Mbarki, M., Moubarik, A. & Oubenali, M. (2023). Future trends in dye removal by metal oxides and their Nano/Composites: A comprehensive review. *Inorganic Chemistry Communications*, 158, 111546. DOI:DOI:10.1016/j.inoche.2023.111546

Khan, Z. R., Khan, M. S., Zulfequar, M. & Shahid Khan, M. (2011). Optical and Structural Properties of ZnO Thin Films Fabricated by Sol-Gel Method. *Materials Sciences and Applications,* 02(05), pp. 340–345. DOI:10.4236/msa.2011.25044

Kumar, P. & Kirthika, K. (2010). Kinetics and equilibrium studies of Zn2+ ions removal from aqueous solutions by use of natural waste. *Electronic Journal of Environmental, Agricultural and Food Chemistry*, 9(1), 264.

Langmuir, I. (1916). The constitution and fundamental properties of solids and liquids. Part I. Solids. *Journal of the American Chemical Society*, 38(11), pp. 2221–2295. DOI:10.1021/ja02268a002

Lemecho, B. A., Sabir, F. K., Andoshe, D. M., Gultom, N. S., Kuo, D. H., Chen, X., Mulugeta, E., Desissa, T. D. & Zelekew, O. A. (2022). Biogenic Synthesis of Cu-Doped ZnO Photocatalyst for the Removal of Organic Dye. *Bioinorganic Chemistry and Applications*. DOI:10.1155/2022/8081494

Liu, Y. X., Liu, Y. C., Shen, D. Z., Zhong, G. Z., Fan, X. W., Kong, X. G., Mu, R. & Henderson, D. O. (2002). Preferred orientation of ZnO nanoparticles formed by post-thermal annealing zinc implanted silica. *Solid State Communications*, 121(9–10), pp. 531–536. DOI:10.1016/S0038-1098(02)00006-6

Mandal, S. K., Das, A. K., Nath, T. K. & Karmakar, D. (2006). Temperature dependence of solubility limits of transition metals (Co, Mn, Fe, and Ni) in ZnO nanoparticles. *Applied Physics Letters*, 89(14). DOI:10.1063/1.2360176

Mehar, S., Khoso, S., Qin, W., Anam, I., Iqbal, A. & Iqbal, K. (2019). Green Synthesis of Zincoxide Nanoparticles from *Peganum harmala*, and its biological potential against bacteria. *Frontiers in Nanoscience and Nanotechnology*, 6(1). DOI:10.15761/fnn.1000188

Mote, D.V., Dargad, J.S. & Dole, B.N. (2013). Effect of Mn Doping Concentration on Structural, Morphological and Optical Studies of ZnO Nano-particles. *Nanoscience and Nanoengineering*, 1(2), pp. 116–122. DOI:10.13189/nn.2013.010204

Owoeye, S. S., Toludare, T. S., Isinkaye, O. E. & Kingsley, U. (2019). Influence of waste glasses on the physico-mechanical behavior of porcelain ceramics. *Boletin de la Sociedad Espanola de Ceramica y Vidrio*, 58(2), pp. 77–84). DOI:10.1016/j.bsecv.2018.07.002

Paksamut, J. & Boonsong, P. (2018). *Removal of Copper(II) Ions in Aqueous Solutions Using Tannin-Rich Plants as Natural Bio-Adsorbents*. IOP Conference Series: Materials Science and Engineering, 317(1). DOI:10.1088/1757-899X/317/1/012058

Paraguay, F., Estrada, W., Acosta, D. R., Andrade, E. & Miki-Yoshida, M. (1999). Growth, structure and optical characterization of high quality ZnO thin films obtained by spray pyrolysis. *Thin Solid Films*, 350, pp. 192–202.

Park, D., Lim, S. R., Yun, Y. S. & Park, J. M. (2008). Development of a new Cr(VI)-biosorbent from agricultural biowaste. *Bioresource Technology*, 99(18), pp. 8810–8818. DOI:10.1016/J.BIORTECH.2008.04.042

Seetawan, U., Jugsujinda, S., Seetawan, T., Ratchasin, A., Euvananont, C., Junin, C., Thanachayanont, C. & Chainaronk, P. (2011). Effect of Calcinations Temperature on Crystallography and Nanoparticles in ZnO Disk. *Materials Sciences and Applications*, 02(09), pp. 1302–1306. DOI:10.4236/msa.2011.29176

Shaba, E. Y., Jacob, J. O., Tijani, J. O. & Suleiman, M. A. T. (2021). A critical review of synthesis parameters affecting the properties of zinc oxide nanoparticle and its application in wastewater treatment. *Applied Water Science*. 11, 48. DOI:10.1007/s13201-021-01370-z

Sharaf, G. & Hassan, H. (2014). Removal of copper ions from aqueous solution using silica derived from rice straw: Comparison with activated charcoal. *International Journal of Environmental Science and Technology*, 11(6), pp. 1581–1590. DOI:10.1007/s13762-013-0343-8

Singh, B., Shrivastava, S. B. & Ganesan, V. (2016). Effects of Mn Doping on Zinc Oxide Films Prepared by Spray Pyrolysis Technique. *International Journal of Nanoscience*, 15(3), 1650024-1–8. DOI:10.1142/S0219581X16500241

Solmaz, A., Turna, T. & Baran, A. (2024). Ecofriendly synthesis of selenium nanoparticles using agricultural Citrus fortunella waste and decolourization of crystal violet from aqueous solution. *The Canadian Journal of Chemical Engineering*, 102(6), pp. 2051–2067. DOI:10.1002/cjce.25179

Sriram, S., Lalithambika, K.C. & Thayumanavan, A. (2017). Experimental and theoretical investigations of photocatalytic activity of Cu doped ZnO nanoparticles. *Optik*, 139, pp. 299–308. DOI:10.1016/J.IJLEO.2017.04.013

Taha, A. A., Ahmed, A. M., Abdel Rahman, H. H., Abouzeid, F.

M. & Abdel Maksoud, M. O. (2017). Removal of nickel ions by adsorption on nano-bentonite: Equilibrium, kinetics, and thermodynamics. *Journal of Dispersion Science and Technology*, 38(5), pp. 757–767. DOI:10.1080/01932691.2016.1194211

Theyvaraju, D. & Muthukumaran, S. (2015). Preparation, structural, photoluminescence and magnetic studies of Cu doped ZnO nanoparticles co-doped with Ni by sol–gel method. *Physica E: Low-Dimensional Systems and Nanostructures*, 74, pp. 93–100. DOI:10.1016/J.PHYSE.2015.06.012

Trari, M., Töpfer, J., Dordor, P., Grenier, J. C., Pouchard, M. & Doumerc, J. P. (2005). Preparation and physical properties of the solid solutions Cu 1+xMn1-xO2 (0≤x≤0.2). *Journal of Solid State Chemistry*, 178(9), pp. 2751–2758. DOI:10.1016/j.jssc.2005.06.009

Ullah, I., Rauf, A., Khalil, A. A., Luqman, M., Islam, M. R., Hemeg, H. A., Ahmad, Z., Al-Awthan, Y. S., Bahattab, O. & Quradha, M. M. (2024). *Peganum harmala* L. extract-based Gold (Au) and Silver (Ag) nanoparticles (NPs): Green synthesis, characterization, and assessment of antibacterial and antifungal properties. *Food Science and Nutrition*. 12(6), pp.4459-4472. DOI:10.1002/fsn3.4112

Yang, Z., Ye, Z., Xu, Z. & Zhao, B. (2009). Effect of the morphology on the optical properties of ZnO nanostructures. *Physica E: Low-Dimensional Systems and Nanostructures*, 42(2), pp. 116–119. DOI:10.1016/j.physe.2009.09.010

Yildirimcan, S., Ocakoglu, K., Erat, S., Emen, F. M., Repp, S. & Erdem, E. (2016). The effect of growing time and Mn concentration on the defect structure of ZnO nanocrystals: X-ray diffraction, infrared and EPR spectroscopy. *RSC Advances*, 6(45), pp. 39511–39521. DOI:10.1039/c6ra04071c

Zafar, M. N., Dar, Q., Nawaz, F., Zafar, M. N., Iqbal, M. & Nazar, M. F. (2019). Effective adsorptive removal of azo dyes over spherical ZnO nanoparticles. *Journal of Materials Research and Technology*, 8(1), pp. 713–725. DOI:10.1016/j.jmrt.2018.06.002

Zhu, Z., Zhao, S. & Wang, C. (2022). Antibacterial, Antifungal, Antiviral, and Antiparasitic Activities of *Peganum harmala* and Its Ingredients: A Review. *MDPI Molecules*, 27(13). DOI:10.3390/molecules27134161